



Since January 2020 Elsevier has created a COVID-19 resource centre with free information in English and Mandarin on the novel coronavirus COVID-19. The COVID-19 resource centre is hosted on Elsevier Connect, the company's public news and information website.

Elsevier hereby grants permission to make all its COVID-19-related research that is available on the COVID-19 resource centre - including this research content - immediately available in PubMed Central and other publicly funded repositories, such as the WHO COVID database with rights for unrestricted research re-use and analyses in any form or by any means with acknowledgement of the original source. These permissions are granted for free by Elsevier for as long as the COVID-19 resource centre remains active.



Contents lists available at ScienceDirect

European Journal of Medicinal Chemistry

journal homepage: <http://www.elsevier.com/locate/ejmech>

Research paper

Discovery of unsymmetrical aromatic disulfides as novel inhibitors of SARS-CoV main protease: Chemical synthesis, biological evaluation, molecular docking and 3D-QSAR study



Li Wang^{a,1}, Bo-Bo Bao^{b,c,1}, Guo-Qing Song^a, Cheng Chen^{b,c,**}, Xu-Meng Zhang^a,
Wei Lu^a, Zefang Wang^{b,c}, Yan Cai^{b,c}, Shuang Li^{b,c}, Sheng Fu^{b,c}, Fu-Hang Song^d,
Haitao Yang^{b,c}, Jian-Guo Wang^{a,*}

^a State-Key Laboratory and Research Institute of Elemento-Organic Chemistry, National Pesticide Engineering Research Center, College of Chemistry, Nankai University, Tianjin 300071, China

^b School of Life Sciences, Tianjin University, Tianjin 300072, China

^c Tianjin International Joint Academy of Biotechnology and Medicine, Tianjin 300457, China

^d CAS Key Laboratory of Pathogenic Microbiology and Immunology, Institute of Microbiology, Chinese Academy of Sciences, Beijing 100101, China

ARTICLE INFO

Article history:

Received 27 February 2017

Received in revised form

17 May 2017

Accepted 21 May 2017

Available online 9 June 2017

Keywords:

SARS-CoV M^{pro}

Aromatic disulfide

Molecular docking

In vitro activity

ABSTRACT

The worldwide outbreak of severe acute respiratory syndrome (SARS) in 2003 had caused a high rate of mortality. Main protease (M^{pro}) of SARS-associated coronavirus (SARS-CoV) is an important target to discover pharmaceutical compounds for the therapy of this life-threatening disease. During the course of screening new anti-SARS agents, we have identified that a series of unsymmetrical aromatic disulfides inhibited SARS-CoV M^{pro} significantly for the first time. Herein, 40 novel unsymmetrical aromatic disulfides were synthesized chemically and their biological activities were evaluated *in vitro* against SARS-CoV M^{pro}. These novel compounds displayed excellent IC₅₀ data in the range of 0.516–5.954 μM. Preliminary studies indicated that these disulfides are reversible and competitive inhibitors. A possible binding mode was generated via molecular docking simulation and a comparative field analysis (CoMFA) model was constructed to understand the structure-activity relationships. The present research therefore has provided some meaningful guidance to design and identify anti-SARS drugs with totally new chemical structures.

© 2017 Elsevier Masson SAS. All rights reserved.

1. Introduction

Severe acute respiratory syndrome (SARS) is a highly infective respiratory disease caused by SARS coronavirus (SARS-CoV). Its sudden emergence and rapid outbreak during 2002–2003 had resulted in ~800 deaths among >8000 reported individual cases worldwide [1]. Although the SARS epidemic had been under control for years, reemergence of this threatening illness is still a possible risk and potentially new strains of SARS can be more dangerous than the previous ones. A number of important targets have been recognized to take part in the biological events critical to

SARS-CoV replication, among which a papain-like protease (PL^{pro}) and a chymotrypsin-like protease (3CL^{pro}) are of significant importance to design anti-SARS inhibitors [2]. The 3CL^{pro}, also known as the main protease (M^{pro}), has attracted much attention, which could be revealed from numerous publications about novel inhibitor discovery. Crystal structures of SARS-CoV M^{pro}, either free enzyme alone or in complex with an inhibitor, had been determined to facilitate the structural and functional investigation of this protease [3,4]. The active site of SARS-CoV M^{pro} contains Cys145 and His41 to constitute a catalytic dyad, in which cysteine functions as the common nucleophile in the proteolytic process.

Biological active inhibitors against SARS-CoV M^{pro} have been reported mainly from two different approaches: one is screening large library to identify new active compounds using high-throughput technique, the other is novel inhibitor design based on the substrate structure or active site properties rationally [5]. The inhibitory activities of these compounds were then validated by *in vitro* protease assays. In most cases the kinetic study indicated

* Corresponding author.

** Corresponding author. School of Life Sciences, Tianjin University, Tianjin 300072, China.

E-mail addresses: chengchen@tju.edu.cn (C. Chen), nkwjg@nankai.edu.cn (J.-G. Wang).¹ These two authors contributed equally to this work.

that the inhibitor is involved in an irreversible process by forming a covalent bond with Cys145, while in some other cases the inhibition is actually a reversible behavior. The reported SARS-CoV M^{pro} inhibitors covered a variety of different chemical scaffolds, which contain peptidomimetic compounds, 3-quinoline carboxylic acid derivatives, thiophene-2-carboxylate derivatives, zinc-conjugated compounds, cinaserin, calmodulin, keto-glutamine analogues, anilide, bifunctional boronic acid compounds, isatin derivatives, etacrynic acid derivatives, serine derivatives, trifluoromethyl ketones, acetamides, pyrazolone and quercertins [5–12]. It is a pity that research on drugs and vaccines towards SARS or SARS-like coronavirus has not brought any candidate for clinical use. Hence there still exists an urgent need to discover and identify new SARS-CoV M^{pro} agents, especially those compounds from totally new chemical families, to develop effective therapy against this fatal viral infection.

Disulfide bonds play essential roles for bioactive proteins to keep correct folding [13]. There are a few cases that simple disulfides such as diallyl disulfide and dimethyl disulfide exhibit hypochlorous acid scavenging activity and tyrosinase inhibitory activity (Fig. 1A) [14,15]. The unsymmetrical disulfide compounds are useful tools in the research of dynamic combinatorial chemistry [16]. These compounds have also been reported to display a variety of biological activities. For examples, Turos et al. reported that some unsymmetrical aryl-alkyl disulfides were inhibitors of methicillin-resistant *Staphylococcus aureus* and *Bacillus anthracis* (Fig. 1B) [17], while Khosla and co-workers published some unsymmetrical disulfides that could selectively inhibit extracellular thioredoxin (Fig. 1C) [18]. Yoon et al. showed that some unsymmetrical disulfide compounds were inhibitors of *Mycobacterium tuberculosis* and *Haemophilus influenzae*, by interfering with acetohydroxyacid synthase (AHAS), a key enzyme in the biosynthesis pathway of branched chain amino-acids (Fig. 1D) [19,20]. In the past of our research, we found that some unsymmetrical aromatic disulfides

could inhibit plant AHAS and was useful for herbicide research (Fig. 1E) [21,22].

There are indeed a few reports that some aromatic disulfides exhibit antiviral activity. The virucidal activity of NSC4492 was due to targeting of arenavirus RNA synthesis (Fig. 1F) [23], while 5,5'-dithiobis-2-nitrobenzoic acid (DTNB) had antiviral properties against T-tropic human immunodeficiency virus type 1 (HIV-1) (Fig. 1G) [24]. An antiviral disulfide NSC20625 compound could block interaction between arenavirus Z protein and cellular promyelocytic leukemia protein (Fig. 1H) [25]. However, the antiviral activities against arenavirus might be different from that against coronavirus. There is no evidence that the reported antiviral activities of aromatic disulfides have any direct relationships with SARS-CoV M^{pro} inhibition.

In an effort to discover novel inhibitors of SARS-CoV M^{pro}, we have synthesized a series of novel unsymmetrical aromatic disulfides and evaluated their biological activities in this study. The target compounds could inhibit main protease of SARS-CoV remarkably, with the best IC₅₀ value of 0.516 μM. Subsequent enzymatic kinetics study indicated that the aromatic disulfides acted as reversible and non-competitive inhibitors. Therefore we have demonstrated that unsymmetrical disulfide compounds with aromatic rings are novel inhibitors of SARS-CoV M^{pro} from a totally new chemical family, which will provide helpful information for further drug discovery.

2. Results and discussion

2.1. Chemistry of the target compounds

The target unsymmetrical disulfides were synthesized by the reaction of various substituted 2-mercapto- [1,3,4]oxadiazole, substituted 2-mercapto-thiazole, substituted 2-mercapto-1H-imidazole or substituted 2-mercapto-pyrimidine with substituted

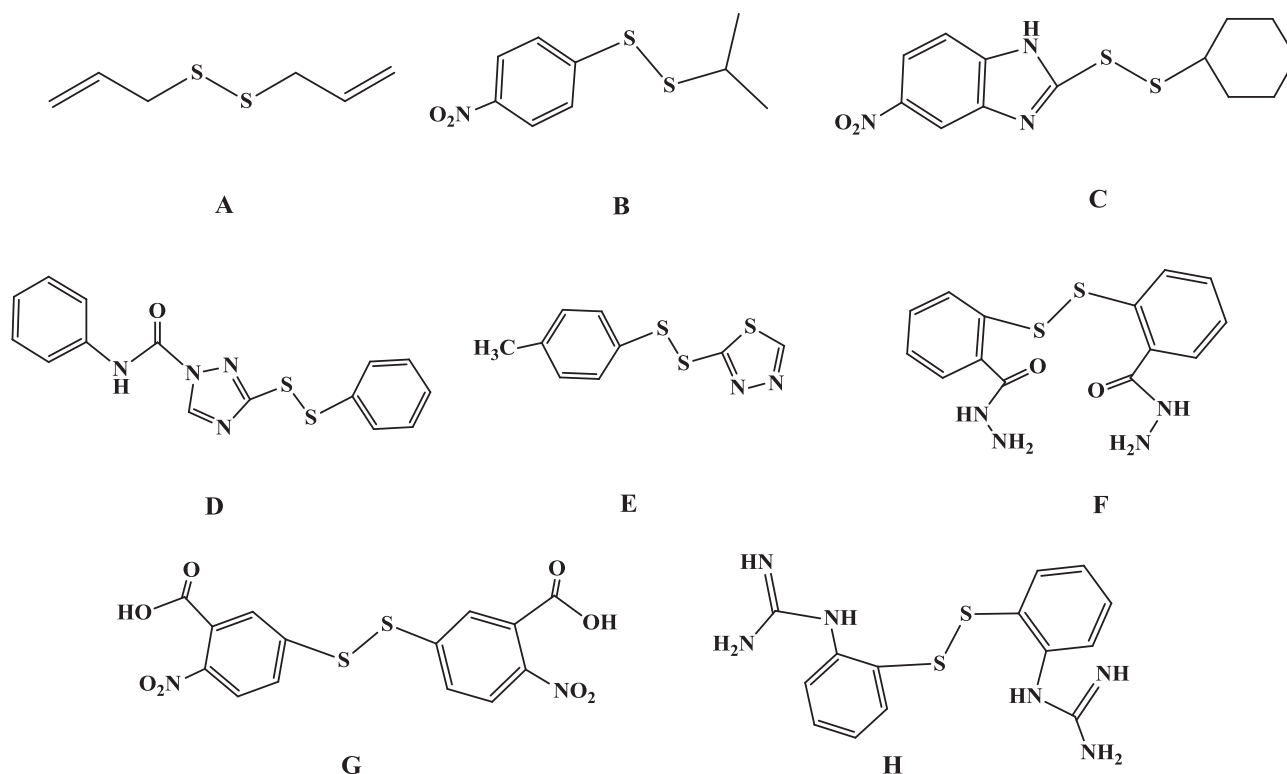


Fig. 1. Different disulfide compounds with various biological activities from literature.

arenesulfonyl chloride in ethyl ether under very mild condition as reported previously [21,22]. It is a quite straightforward nucleophilic substitution, in which the thiol group in the mercapto compound serves as a nucleophilic reagent and attacks the sulfur atom in the arenesulfonyl chloride. Most yields for the reactions were satisfactory, showing that this is a simple and easy procedure to produce unsymmetrical aromatic disulfides, superior to the synthetic route developed by Hahn et al. [26]. In Hahn's paper, moist tetrahydrofuran gave better yields than dried benzene as the solvent for the reaction, so the authors added 5–10 M equivalent of water to the reaction mixture and observed satisfactory yields. Thus, the presence of water was thought to be preferable for the reaction by Hahn et al. [26]. In our synthesis experiment, only ethyl ether was used as the solvent and no additional water was added to the reaction, nevertheless, we observed very high yields for most of the target compounds.

The –S–S– bond had been confirmed in our previous paper [21]. Compound **3-4**, **3-6**, **3-7**, **3-8**, **3-9**, **3-10** and **3-11** were further acetylated from corresponding parent compounds that had been published by us [21]. The molecular structures of the compounds are listed in Table 1. The title compounds were fully characterized by ^1H NMR, ^{13}C NMR and HRMS (Part 1 of the supplementary data for the original figures).

2.2. *In vitro* inhibitory activity of SARS-CoV M^{Pro}

All the synthesized unsymmetrical aromatic disulfides were subjected to the *in vitro* assay of SARS-CoV M^{Pro}. The results are also illustrated in Table 1, expressed by IC_{50} values. It could be seen that the target compounds exhibited encouraging biological potency, with excellent IC_{50} values ranging from 0.516 μM to 5.954 μM (The inhibition curves of all target compounds can be found in part 2 of the supplementary data). This was surprising due to the fact that not any research group had ever identified the disulfide compounds as inhibitors of SARS-CoV M^{Pro}, not to mention such strong inhibition.

Inhibition type of the disulfides was determined by means of enzymatic kinetic study, for which **3-31** and **3-39** were used. From Fig. 2 it can be seen that in the plot of enzyme concentration versus reaction velocity, the lines represent different inhibitor concentrations intersect at a same point, suggesting that the inhibition is actually a reversible action. We then measured the enzymatic velocity of SARS-CoV M^{Pro} versus substrate concentrations in the presence of either **3-31** or **3-39** (Part 3 of the supplementary data). The lines displayed in reciprocal plots intersect at a same point, indicating that both inhibitors serve as a non-competitive inhibitor with $\alpha < 1$ (Part 3 of the supplementary data) [27]. On this basis, the kinetic parameters ($\alpha K_i = 0.20 \mu\text{M}$, $K_i = 0.24 \mu\text{M}$) of **3-31** were determined [28] (Fig. 3), which clearly proved that, the non-competitive inhibitor **3-31** is characterized by smaller equilibrium-binding constant compared to some known inhibitors such as N3 ($K_i = 9.0 \mu\text{M}$) and N9 ($K_i = 6.7 \mu\text{M}$) [3].

Since there is a cysteine in the active site of SARS-CoV M^{Pro} (Cys145), which plays an essential role for the biological activity of this protease, it is possible that the disulfide compound reacts with Cys145 to form a new –S–S– bond and results in a loss of enzyme activity. It is known that, if a disulfide reacts with another thiol to give a new disulfide, the thiols that are parts of the old disulfide can also react directly with this thiol to form the same new disulfide [29]. We tested the biological activities of different aryl thiols derived from our disulfides, and no inhibition of SARS-CoV M^{Pro} could be detected for any of them even at very high concentration. Accordingly it seemed unlikely that Cys145 formed a –S–S– bond by reacting with the target disulfide compounds. Another method to rule out this possibility is to determine the change of the molecular

weight of the protein before and after inhibition [30,31]. If the disulfide compound reacts with Cys145, the molecular weight would have a shift after SARS-CoV M^{Pro} is inhibited, and this is approximately the mass of half moiety of the unsymmetrical disulfide. Bearing this in mind, we measured the molecular weight of protease before and after inhibition by three disulfide compounds with significant structure difference (**3-8**, **3-31** and **3-39**, data shown in part 4 of the supplementary data). However, no such assumed shift in the molecular weight was observed to support this idea.

For another possibility, Khosla et al. had reported selective inhibition of extracellular thioredoxin by unsymmetrical disulfides [18], in which two cysteine residues in a close distance form an intramolecular disulfide bond. After careful analysis of the SARS-CoV M^{Pro} crystal structure (pdb entry 2AMD) [3], no other cysteine residue was found to be in a nearby space of Cys145. In fact not any two cysteine residues are in a reasonable distance to form possible intramolecular disulfide bond. Thus we also denied this probable inhibitory mechanism.

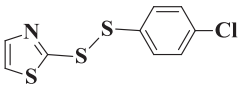
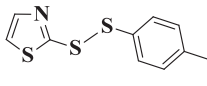
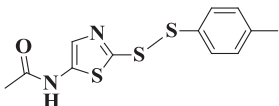
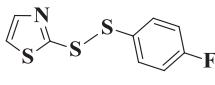
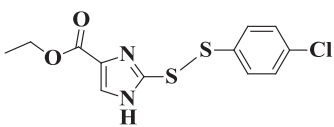
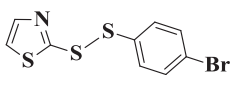
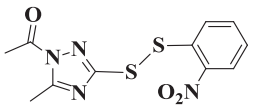
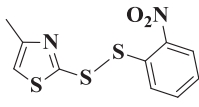
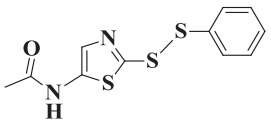
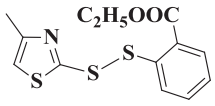
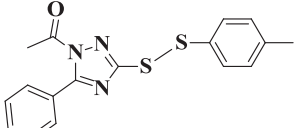
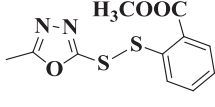
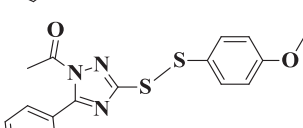
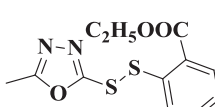
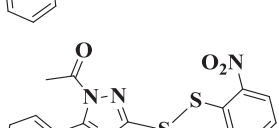
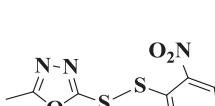
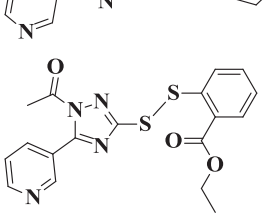
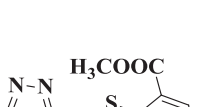
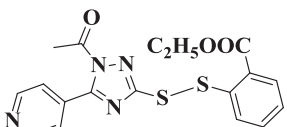
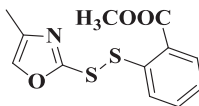
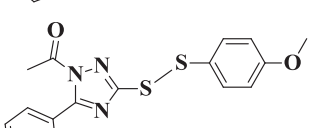
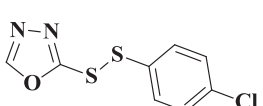
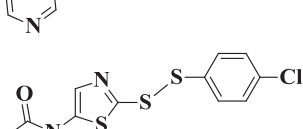
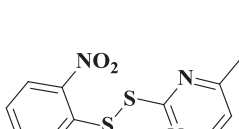
2.3. Molecular docking and three dimensional structure-activity relationships

Since the unsymmetrical aromatic disulfides do not react with the residues of the SARS-CoV M^{Pro}, it means that these compounds act as intact molecules when inhibiting this protease. Therefore, *in silico* molecular docking technique was utilized to predict possible binding modes of the disulfide compounds with SARS-CoV M^{Pro}. In our previous study, we had docked a small library of isatin compounds to the active site of AHAS and probable binding modes were predicted by FlexX [32–37]. Here similar strategy was adopted to carry out database docking. After investigation of the resulting docked conformations, nineteen compounds were found to overlay one another quite well (Part 5 of the supplementary data), while all the other twenty-one compounds were in unreasonable binding space, and they failed to overlay well with one another. Thus, the docked conformations of the nineteen compounds were thought to be the possible binding conformations in this study. Compound **3-31** was chosen to depict the binding mode of the disulfide inhibitors. Fig. 4 is a two-dimensional illustration of the interactions between the inhibitor and the surrounding residues of SARS-CoV M^{Pro} drawn by LIGPLOT [38]. The location of **3-31** has some overlap with the inhibitor N9, the inhibitor in the original pdb file. The compound binds with SARS-CoV M^{Pro} via multiple hydrogen bonding contacts and hydrophobic contacts. Phe140, Leu141, His163, Met165, Glu166 and His172 form hydrophobic interactions with the small molecule, while Asn142, Gly143 and Cys145 form intermolecular H-bond with the inhibitor. The predicted binding mode therefore provides a useful clue to understand the possible molecular basis of these inhibitors.

Comparative field analysis (CoMFA) is a tool to generate 3D contour models to quantitatively analyze the structure-activity relationships of bioactive compounds by steric and electrostatic contributions [39–41]. On the basis of the docked conformation, the molecules in the database were aligned to construct a CoMFA model. Compounds **3-8**, **3-23** and **3-40** were excluded from the database because they were statistical outliers in the training set, that is, the inclusion of any of these molecules did not yield a satisfactory leave-one-out q^2 . The training set without the outliers gave a leave-one-out q^2 of 0.681 when the optimum components was 6, and the non-crossvalidated r^2 was 0.916, with a standard error of estimate of 0.088 and F values of 37.968. The steric and electrostatic contributions were 43.6% and 56.4%, respectively.

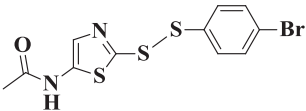
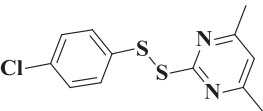
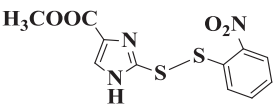
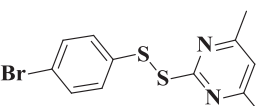
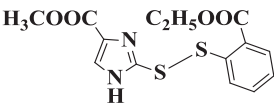
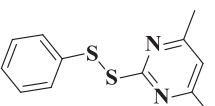
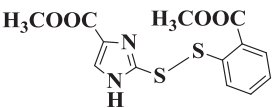
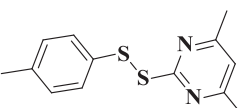
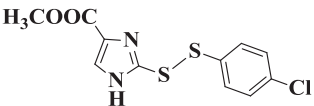
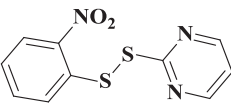
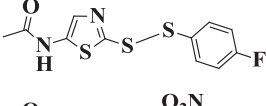
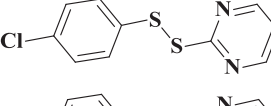
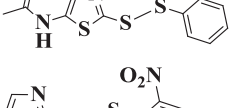
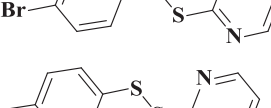
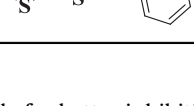
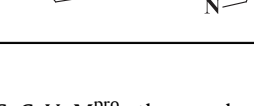
Compound **3-31** was used to illustrate the steric and electrostatic contour maps, together with the neighboring residues in the docked binding pocket (Fig. 5). For the steric contour map, a bulky

Table 1
The novel unsymmetrical aromatic disulfide compounds and their SARS-CoV M^{pro} inhibitory activities (IC_{50}).

Entry no.	Chemical structure	IC_{50} (μ M)	Entry no.	Chemical structure	IC_{50} (μ M)
3-1		1.871 ± 0.071	3-21		1.250 ± 0.023
3-2		2.803 ± 0.052	3-22		2.211 ± 0.152
3-3		3.675 ± 0.193	3-23		3.321 ± 0.068
3-4		3.130 ± 0.052	3-24		2.555 ± 0.270
3-5		1.506 ± 0.184	3-25		2.452 ± 0.126
3-6		4.344 ± 0.538	3-26		1.679 ± 0.042
3-7		4.100 ± 0.832	3-27		1.557 ± 0.116
3-8		1.762 ± 0.044	3-28		1.713 ± 0.052
3-9		5.654 ± 0.259	3-29		1.118 ± 0.132
3-10		4.511 ± 0.105	3-30		1.264 ± 0.033
3-11		5.794 ± 0.050	3-31		0.516 ± 0.060
3-12		2.626 ± 0.082	3-32		0.921 ± 0.060

(continued on next page)

Table 1 (continued)

Entry no.	Chemical structure	IC ₅₀ (μM)	Entry no.	Chemical structure	IC ₅₀ (μM)
3-13		1.651 ± 0.048	3-33		1.437 ± 0.053
3-14		2.075 ± 0.016	3-34		1.121 ± 0.060
3-15		5.954 ± 0.363	3-35		1.991 ± 0.086
3-16		3.957 ± 0.190	3-36		1.495 ± 0.055
3-17		4.126 ± 0.094	3-37		0.883 ± 0.028
3-18		2.565 ± 0.075	3-38		0.684 ± 0.012
3-19		1.947 ± 0.508	3-39		0.697 ± 0.053
3-20		2.029 ± 0.488	3-40		1.522 ± 0.214

group is favorable for better inhibition in the green contour region and such a group is likely to decrease the activity in the yellow contour space. The green maps are mostly in three bulks: one formed by Ser1and Leu141, one formed by Asn142 and Gly143 and the last one formed by Ser144 and Cys145; whereas the yellow maps are just located in a space nearby Gly143. For the electrostatic contour map, in the blue contour region, an increase in the positive charge will lead to an increase of activity, yet in the red contour region, negative charge is favorable to enhance the activity. The blue map is in a region surrounded by Leu27, Gly143, Ser144 and Cys145, whereas the red maps are in three cavities: one formed by Leu141 and Asn142, one formed by Ser144, Cys145 and Met165 and the last one formed by Asn142 and Gly143. The 3D CoMFA maps have afforded important structural features of the unsymmetrical aromatic disulfides from steric and electrostatic views, which is valuable for further design and discovery of more potent inhibitors.

3. Conclusion

The lack of effective anti-SARS agents makes it a possible danger when SARS breaks out sometime in the future, numerous people will be killed again. Therefore it is still an urgent demand to discover novel anti-SARS inhibitors to combat this deadly disease. SARS CoV M^{Pro} is an important target for the design of therapeutically useful drugs. In the present study, in an effort to develop non-peptidic anti-SARS inhibitors, we have identified for the first time, that some unsymmetrical aromatic disulfides are excellent

inhibitors of SARS CoV M^{Pro}, the mechanism of which seems distinct as they are reversible and competitive inhibitors. This suggests that the unsymmetrical disulfides are promising lead compounds identification and development of a new family of biologically active anti-SARS agents. A possible binding model of the disulfide inhibitor was built by molecular docking, and a CoMFA model was constructed subsequently to point out the structural features of these novel inhibitors of SARS CoV M^{Pro}. Based on this information, further structural modifications are ongoing for better pharmaceutical compounds. The Lipinski rules will also be utilized to help to develop compounds with a final *in vivo* activity [42]. We are also trying to co-crystallize the protease and the best inhibitor, to gain insight into a real binding mode and explain the molecular basis of these compounds.

4. Experimental section

4.1. General synthesis and instruments

Various heterocyclic aromatic thiols **1** were commercial procured from 5A Pharmatech (China), Apichemical (China), Aldrich and ACES pharma, which were all >95% purity grade. All solvents and liquid reagents were dried in advance using standard methods and distilled before use. Substituted arenesulfonyl chlorides **2** were synthesized as described in our previous publications [21,22]. Synthetic methods for compounds **3'** had been reported and these parent compounds for **3-4**, **3-6**, **3-7**, **3-8**, **3-9**, **3-10** and **3-11** had also

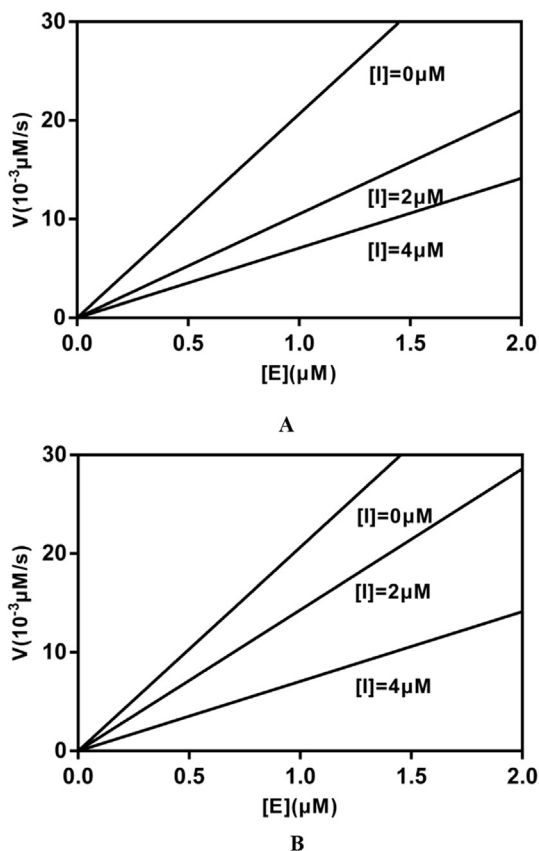


Fig. 2. Plot of enzyme concentration versus reaction velocity for enzymatic kinetic study of 3-31 (A) and 3-39 (B).

been fully characterized before [21]. Melting points were determined using an X-4 melting apparatus and were uncorrected. ^1H NMR spectra and ^{13}C NMR were obtained using a 400 MHz Varian Mercury Plus 400 spectrometer. The chemical shift values (δ) for the NMR spectra were reported as parts per million (ppm), using deuterated chloroform (CDCl_3) or dimethyl sulfoxide ($\text{DMSO}-d_6$) as the solvent and tetramethylsilane (TMS) as an internal reference standard. Mass spectra were recorded on a Thermo Finnigan LCQ Advantage LC/mass detector instrument.

4.2. Synthesis of the target compounds (Scheme 1)

Heterocyclic aromatic thiols (**1**, 5 mmol) was added to a solution of freshly prepared arenesulfonyl chlorides (**2**, 5 mmol) in 25 mL of anhydrous ethyl ether at room temperature. The mixture was then stirred for 5 h at the same temperature, after that the solvent was removed under reduced pressure. Products **3** (**3'** for **3-4**, **3-6**, **3-7**, **3-8**, **3-9**, **3-10** and **3-11**) were purified by column chromatography in 75–95% yields.

4.3. Synthesis of the compounds 3-4, 3-6, 3-7, 3-8, 3-9, 3-10 and 3-11 (Scheme 2)

Unsymmetrical aromatic disulfide (**3'**, 5 mmol) was added to 10 mL of acetic anhydride. The reaction mixture was stirred for 0.5 h at 60°C and then 200 mL water was added to the mixture. The pH value was adjusted by sodium bicarbonate to 7–8. The product was extracted by ethyl acetate and the solvent was removed under reduced pressure. The target compounds were finally purified by

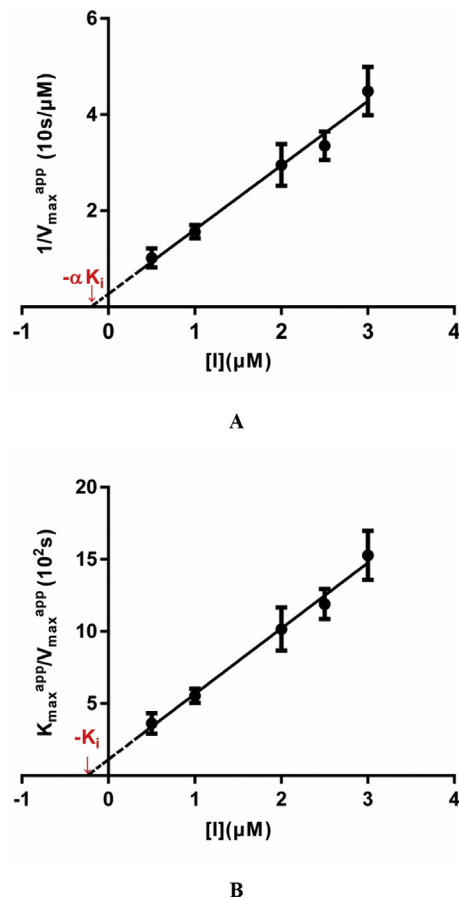


Fig. 3. Secondary plots for the determination of the kinetic constants (K_i and αK_i) of inhibitor 3-31 as a non-competitive inhibitor. The values of αK_i (A) and K_i (B) are calculated from the x intercept.

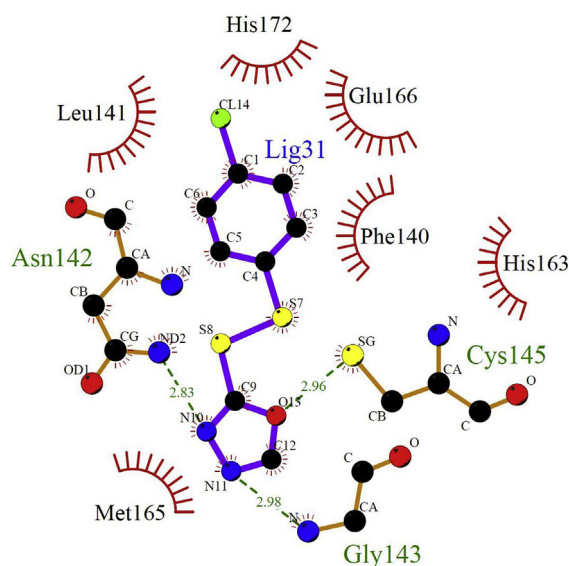


Fig. 4. LIGPLOT 2D representation of 3-31 bound with SARS CoV Mpro from FlexX docking. The hydrogen bonds between the enzyme and the inhibitor are shown as green dashed lines, and distances are in Å units. Amino acid residues that are within van der Waals contact of the inhibitor are shown as red arcs. (For interpretation of the references to colour in this figure legend, the reader is referred to the web version of this article.)

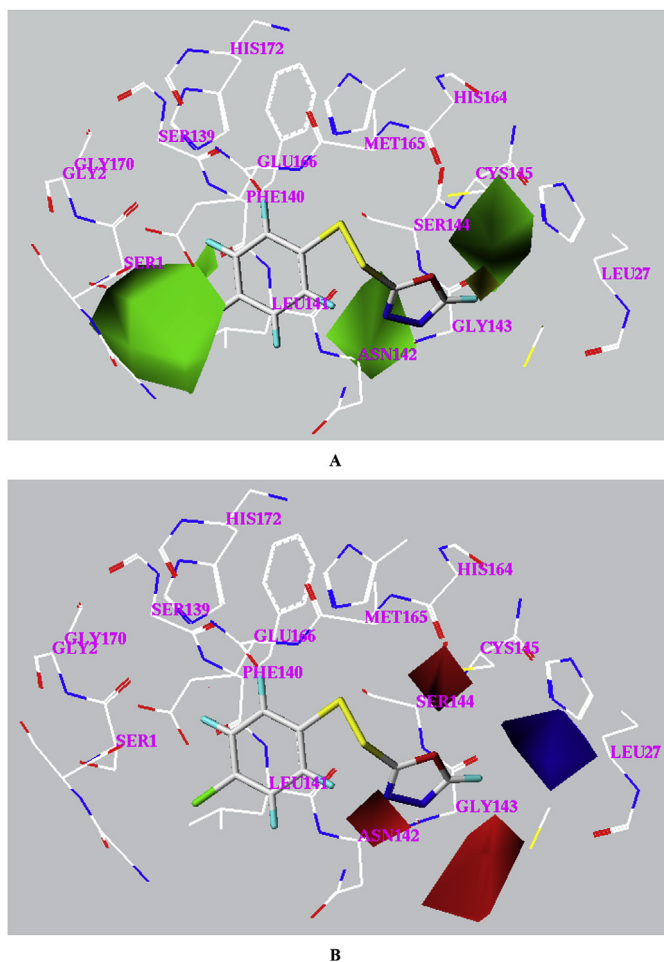


Fig. 5. Steric contour map (A) and electrostatic contour map (B) for the CoMFA model. Sterically favored and disfavored regions are shown in green and yellow in map A. Electrostatic favored and disfavored regions are shown in blue and red in map B. (For interpretation of the references to colour in this figure legend, the reader is referred to the web version of this article.)

column chromatography in 87–95% yields.

4.4. Characterization of the target compounds

4.4.1. 2-((4-chlorophenyl)disulfanyl)thiazole (3-1)

Yield 89%; m.p.: 114–116 °C; yellow solid; $^1\text{H NMR}$ (400 MHz, $\text{DMSO-}d_6$), δ 7.62 (d, $J = 8.5$ Hz, 2H, ArH), 7.47 (d, $J = 8.5$ Hz, 2H, ArH), 7.31 (s, 1H, NCH), 6.99 (d, $J = 4.3$ Hz, 1H, SCH); $^{13}\text{C NMR}$ (101 MHz, $\text{DMSO-}d_6$), δ 134.8, 132.2, 129.3, 121.9, 114.20, 99.7; HRMS(MALDI) m/z : calculated for $\text{C}_9\text{H}_6\text{ClNS}_3$ 259.9423, found 259.9420 $[\text{M} + \text{H}]^+$.

4.4.2. *N*-2-(*p*-tolylidysulfanyl)thiazol-5-yl)acetamide (3-2)

Yield 91%; m.p.: 113–115 °C; yellow solid; $^1\text{H NMR}$ (400 MHz, $\text{DMSO-}d_6$), δ 11.70 (s, 1H, NH), 7.50 (d, $J = 6.5$ Hz, 2H, ArH), 7.47 (s, 1H, CH), 7.26 (d, $J = 7.8$ Hz, 2H, ArH), 2.32 (s, 3H, CH_3), 2.10 (s, 3H, CH_3); $^{13}\text{C NMR}$ (101 MHz, $\text{DMSO-}d_6$), 167.6, 154.1, 138.9, 132.3, 130.6, 130.0, 128.4, 22.6, 21.1; HRMS(MALDI) m/z : calculated for $\text{C}_{12}\text{H}_{12}\text{N}_2\text{OS}_3$ 297.0185, found 297.0185 $[\text{M} + \text{H}]^+$.

4.4.3. Ethyl 2-((4-chlorophenyl)disulfanyl)-1*H*-imidazole-4-carboxylate (3-3)

Yield 87%; m.p.: 100–102 °C; yellow solid; $^1\text{H NMR}$ (400 MHz,

$\text{DMSO-}d_6$), δ 7.98 (s, 1H), 7.64 (d, $J = 8.6$ Hz, 2H, ArH), 7.49 (d, $J = 8.6$ Hz, 2H, ArH), 4.24 (q, $J = 7.0$ Hz, 2H, CH_2CH_3), 1.27 (t, $J = 7.1$ Hz, 3H, CH_2CH_3); $^{13}\text{C NMR}$ (101 MHz, $\text{DMSO-}d_6$), δ 161.1, 132.9, 131.7, 128.7, 117.1, 116.9, 60.5, 14.7; HRMS(MALDI) m/z : calculated for $\text{C}_{12}\text{H}_{11}\text{ClN}_2\text{O}_2\text{S}_2$ 315.0022, found 315.0021 $[\text{M} + \text{H}]^+$.

4.4.4. 1-(5-Methyl-3-((2-nitrophenyl)disulfanyl)-1*H*-1,2,4-triazol-1-yl)ethanone (3-4)

Yield 90%; m.p.: 157–159 °C; yellow solid; $^1\text{H NMR}$ (400 MHz, $\text{DMSO-}d_6$), δ 8.31 (d, $J = 8.2$ Hz, 1H), 8.24 (d, $J = 8.2$ Hz, 1H), 7.91 (t, $J = 7.7$ Hz, 1H), 7.58 (t, $J = 7.8$ Hz, 1H), 2.59 (s, 3H), 2.55 (s, 3H); $^{13}\text{C NMR}$ (101 MHz, $\text{DMSO-}d_6$), δ 169.3, 157.8, 157.3, 144.9, 135.6, 134.3, 127.9, 126.6, 23.5, 15.6; HRMS(MALDI) m/z : calculated for $\text{C}_{11}\text{H}_{10}\text{N}_4\text{O}_3\text{S}_2$ 311.0273, found 311.0261 $[\text{M} + \text{H}]^+$.

4.4.5. *N*-2-(phenylidysulfanyl)thiazol-5-yl)acetamide (3-5)

Yield 89%; m.p.: 108–110 °C; yellow solid; $^1\text{H NMR}$ (400 MHz, $\text{DMSO-}d_6$), δ 11.79 (s, 1H, NH), 7.64 (t, $J = 8.6$ Hz, 2H, ArH), 7.53 (d, $J = 8.5$ Hz, 1H, ArH), 7.51–7.42 (m, 2H, ArH), 7.39 (d, $J = 7.1$ Hz, 1H, ArH), 2.10 (s, 3H, CH_3); $^{13}\text{C NMR}$ (101 MHz, $\text{DMSO-}d_6$), δ 167.6, 139.4, 137.2, 130.8, 130.0, 129.9, 129.0, 128.8, 128.42, 22.6; HRMS(MALDI) m/z : calculated for $\text{C}_{11}\text{H}_{10}\text{N}_2\text{OS}_3$ 283.0029, found 283.0031 $[\text{M} + \text{H}]^+$.

4.4.6. 1-(5-Phenyl-3-(*p*-tolylidysulfanyl)-1*H*-1,2,4-triazol-1-yl)ethanone (3-6)

Yield 92%; m.p.: 112–114 °C; white solid; $^1\text{H NMR}$ (400 MHz, $\text{DMSO-}d_6$), δ 8.35 (d, $J = 17.6$ Hz, 1H), 8.00 (d, $J = 8.1$ Hz, 2H), 7.79 (d, $J = 7.6$ Hz, 3H), 7.56 (t, $J = 7.6$ Hz, 1H), 7.27 (s, 2H), 2.72 (s, 3H), 2.33 (s, 3H); $^{13}\text{C NMR}$ (101 MHz, $\text{DMSO-}d_6$), δ 135.4, 129.4, 128.9, 128.1, 126.2, 125.8, 129.5, 22.2, 20.8; HRMS(MALDI) m/z : calculated for $\text{C}_{17}\text{H}_{15}\text{N}_3\text{OS}_2$ 342.0729, found 342.0734 $[\text{M} + \text{H}]^+$.

4.4.7. 1-(3-((4-methoxyphenyl)disulfanyl)-5-phenyl-1*H*-1,2,4-triazol-1-yl)ethanone (3-7)

Yield 91%; m.p.: 133–135 °C; white solid; $^1\text{H NMR}$ (400 MHz, $\text{DMSO-}d_6$), δ 8.11 (s, 2H), 7.70 (d, $J = 7.3$ Hz, 2H), 7.38 (s, 3), 6.73 (d, $J = 7.2$ Hz, 2H), 3.65 (s, 3H), 2.58 (s, 3H); $^{13}\text{C NMR}$ (101 MHz, $\text{DMSO-}d_6$), δ 169.3, 161.9, 161.2, 158.9, 134.8, 129.9, 129.3, 128.5, 127.1, 124.8, 115.0, 55.2, 22.5; HRMS(MALDI) m/z : calculated for $\text{C}_{17}\text{H}_{15}\text{N}_3\text{O}_2\text{S}_2$ 358.0683, found 358.0685 $[\text{M} + \text{H}]^+$.

4.4.8. 1-(3-((2-nitrophenyl)disulfanyl)-5-(pyridin-3-yl)-1*H*-1,2,4-triazol-1-yl)ethanone (3-8)

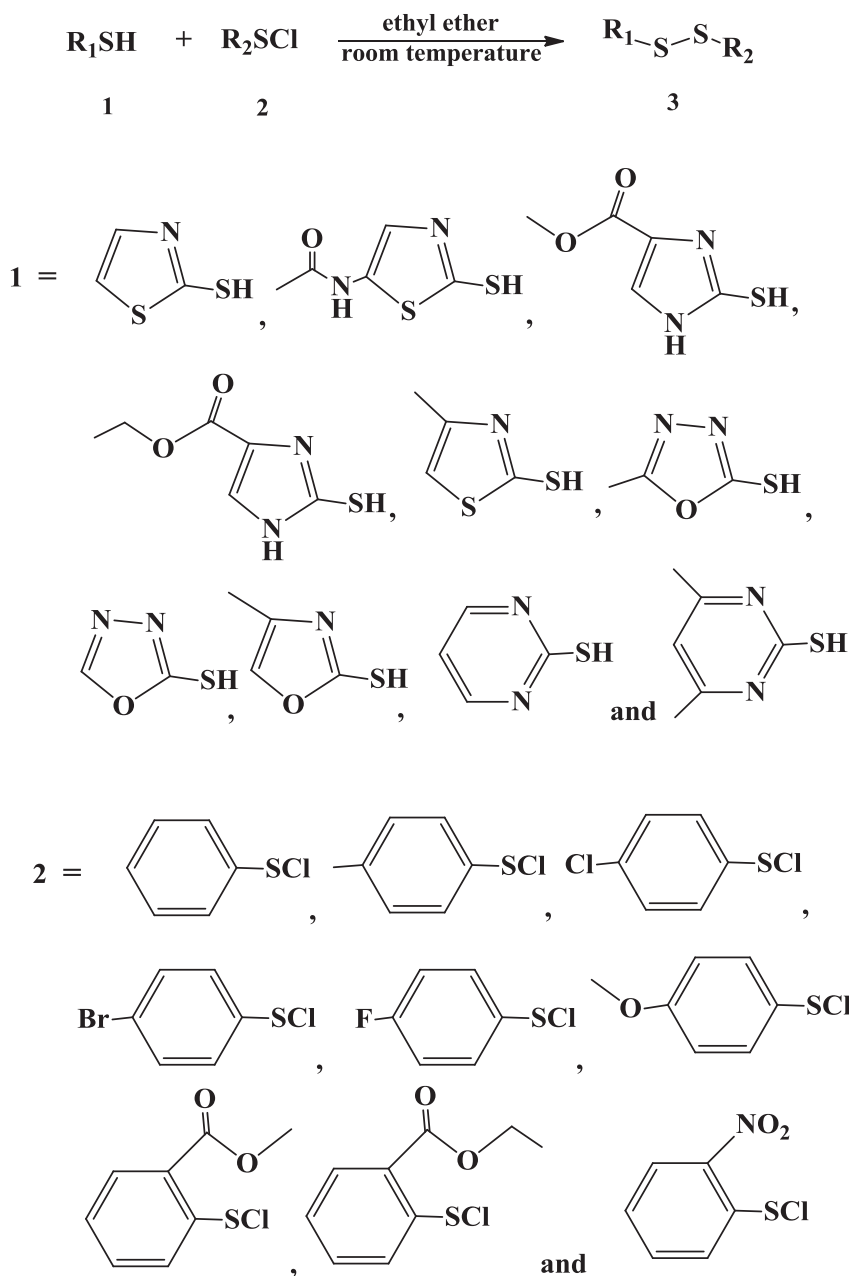
Yield 89%; m.p.: 186–188 °C; yellow solid; $^1\text{H NMR}$ (400 MHz, CDCl_3), δ 8.64 (d, $J = 4.6$ Hz, 1H), 7.95 (d, $J = 4.8$ Hz, 1H), 7.70–7.42 (m, 1H), 7.33 (d, $J = 8.4$ Hz, 2H), 7.21 (d, $J = 8.7$ Hz, 3H), 3.06 (s, 3H); $^{13}\text{C NMR}$ (101 MHz, CDCl_3), δ 174.9, 150.1, 135.3, 129.9, 129.5, 129.3, 127.5, 120.7, 46.0, 29.7; HRMS(MALDI) m/z : calculated for $\text{C}_{15}\text{H}_{11}\text{N}_5\text{O}_3\text{S}_2$ 374.0381, found 374.0380 $[\text{M} + \text{H}]^+$.

4.4.9. Ethyl 2-((1-acetyl-5-(pyridin-3-yl)-1*H*-1,2,4-triazol-3-yl)disulfanyl)benzoate (3-9)

Yield 92%; m.p.: 128–130 °C; white solid; $^1\text{H NMR}$ (400 MHz, $\text{DMSO-}d_6$), δ 9.10 (s, 1H), 8.66 (s, 1H), 8.26 (d, $J = 7.8$ Hz, 2H), 8.00 (d, $J = 7.5$ Hz, 1H), 7.75 (s, 1H), 7.57 (d, $J = 7.2$ Hz, 1H), 7.41 (s, 1H), 4.22 (q, 2H), 2.50 (s, 3H), 1.33 (t, $J = 7.1$ Hz, 3H); $^{13}\text{C NMR}$ (101 MHz, $\text{DMSO-}d_6$), δ 150.1, 135.1, 133.6, 130.9, 129.5, 129.3, 120.7, 45.9, 29.7, 22.5, 8.7; HRMS(MALDI) m/z : calculated for $\text{C}_{18}\text{H}_{16}\text{N}_4\text{O}_3\text{S}_2$ 401.0736, found 401.0746 $[\text{M} + \text{H}]^+$.

4.4.10. Ethyl 2-((1-acetyl-5-(pyridin-4-yl)-1*H*-1,2,4-triazol-3-yl)disulfanyl)benzoate (3-10)

Yield 95%; m.p.: 130–132 °C; white solid; $^1\text{H NMR}$ (400 MHz, $\text{DMSO-}d_6$), δ 9.10 (s, 1H), 8.66 (s, 1H), 8.26 (d, $J = 7.8$ Hz, 2H), 8.00 (d,



Scheme 1. Synthesis route of the target unsymmetrical aromatic disulfide compounds.

$J = 7.5$ Hz, 1H), 7.75 (t, $J = 7.6$ Hz, 1H), 7.54 (s, 1H), 7.41 (t, $J = 7.2$ Hz, 1H), 4.34 (q, $J = 7.1$ Hz, 2H), 2.50 (s, 3H), 1.33 (t, $J = 7.1$ Hz, 3H); ^{13}C NMR (101 MHz, DMSO- d_6), δ 167.9, 150.1, 135.1, 133.6, 130.9, 129.5, 129.3, 120.7, 45.9, 29.7, 8.6; HRMS(MALDI) m/z : calculated for $\text{C}_{18}\text{H}_{16}\text{N}_4\text{O}_3\text{S}_2$ 401.0737, found 401.0746 [M + H] $^+$.

4.4.11. 1-(3-((4-methoxyphenyl)disulfanyl)-5-(pyridin-3-yl)-1H-1,2,4-triazol-1-yl)ethanone (3-11)

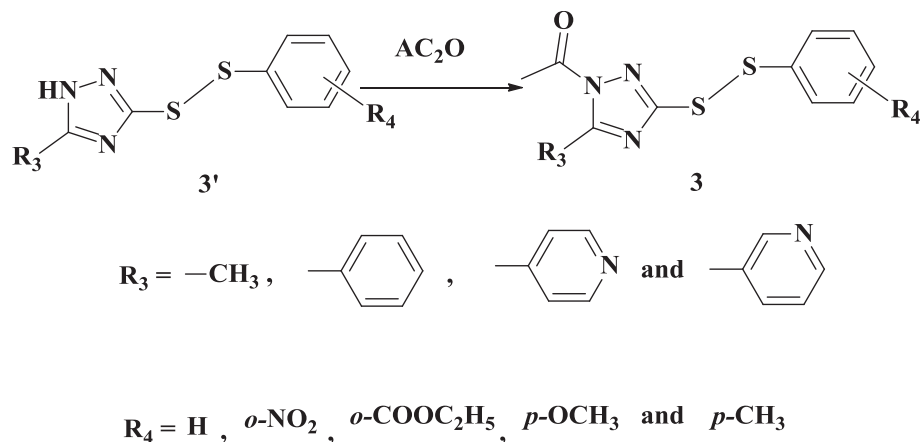
Yield 87%; m.p.: 113–115 °C; white solid; ^1H NMR (400 MHz, DMSO- d_6), δ 9.32 (d, $J = 37.6$ Hz, 1H), 8.53 (d, $J = 5.9$ Hz, 2H), 7.72 (d, $J = 8.5$ Hz, 1H), 7.54–7.27 (m, 2H), 6.76 (d, $J = 8.8$ Hz, 2H), 3.70 (s, 3H), 2.64 (s, 3H); ^{13}C NMR (101 MHz, DMSO- d_6), δ 161.0, 160.3, 150.9, 148.3, 135.8, 134.0, 123.7, 115.0, 114.7, 55.4, 29.7; HRMS(MALDI) m/z : calculated for $\text{C}_{16}\text{H}_{14}\text{N}_4\text{O}_2\text{S}_2$ 359.0630, found 359.0639 [M + H] $^+$.

4.4.12. N-(2-((4-chlorophenyl)disulfanyl)thiazol-5-yl)acetamide (3-12)

Yield 94%; m.p.: 127–129 °C; yellow solid; ^1H NMR (400 MHz, DMSO- d_6), δ 11.73 (s, 1H, NH), 7.65 (d, $J = 8.6$ Hz, 2H, ArH), 7.52 (d, $J = 8.5$ Hz, 2H, ArH), 7.48 (s, 1H, CH), 2.10 (s, 3H, CH $_3$); ^{13}C NMR (101 MHz, DMSO- d_6), δ 167.6, 153.1, 152.0, 139.3, 134.4, 133.6, 130.8, 129.9, 128.5, 22.6; HRMS(MALDI) m/z : calculated for $\text{C}_{11}\text{H}_9\text{ClN}_2\text{OS}_3$ 316.9639, found 316.9641 [M + H] $^+$.

4.4.13. N-(2-((4-bromophenyl)disulfanyl)thiazol-5-yl)acetamide (3-13)

Yield 93%; m.p.: 123–125 °C; yellow solid; ^1H NMR (400 MHz, DMSO- d_6), δ 11.72 (s, 1H, NH), 7.65 (d, $J = 8.6$ Hz, 2H, ArH), 7.58 (d, $J = 8.6$ Hz, 2H, ArH), 7.48 (s, 1H, CH), 2.10 (s, 3H, CH $_3$); ^{13}C NMR (101 MHz, DMSO- d_6), δ 167.5, 167.0, 152.0, 139.6, 132.4, 130.5, 128.0, 121.6, 22.2; HRMS(MALDI) m/z : calculated for $\text{C}_{11}\text{H}_9\text{BrN}_2\text{OS}_3$



Scheme 2. Synthesis route of the target unsymmetrical aromatic disulfide compounds (**3-4**, **3-6**, **3-7**, **3-8**, **3-9**, **3-10** and **3-11**).

360.9132, found 360.9128 [M + H]⁺.

4.4.14. Methyl 2-((2-nitrophenyl)disulfanyl)-1H-imidazole-4-carboxylate (3-14**)**

Yield 88%; m.p.: 160–163 °C; yellow solid; ¹H NMR (400 MHz, DMSO-*d*₆), δ 8.51 (d, *J* = 8.2 Hz, 1H, ArH), 8.31 (dd, *J* = 8.2, 1.1 Hz, 1H, ArH), 7.98 (s, 1H), 7.96 (s, 1H, NHCH), 7.58 (dd, *J* = 11.4, 4.1 Hz, 1H, ArH), 3.74 (s, 3H, OCH₃); ¹³C NMR (101 MHz, DMSO-*d*₆), δ 158.9, 151.1, 139.8, 137.7, 131.2, 130.5, 129.4, 125.2, 124.4, 122.2, 53.0; HRMS(MALDI) *m/z*: calculated for C₁₁H₉N₃O₄S₂ 312.0107, found 312.0112 [M + H]⁺.

4.4.15. Methyl 2-((2-ethoxycarbonyl)phenyl)disulfanyl)-1H-imidazole-4-carboxylate (3-15**)**

Yield 92%; m.p.: 93–95 °C; yellow solid; ¹H NMR (400 MHz, DMSO-*d*₆), δ 8.34 (d, *J* = 8.2 Hz, 1H, ArH), 8.03–7.96 (m, 1H, ArH), 7.96 (s, 1H, NHCH), 7.79–7.66 (m, 1H, ArH), 7.41 (t, *J* = 7.5 Hz, 1H, ArH), 4.32 (q, *J* = 7.1 Hz, 2H, CH₂CH₃), 3.74 (s, 3H, OCH₃), 1.32 (t, *J* = 7.1 Hz, 3H, CH₂CH₃); ¹³C NMR (101 MHz, DMSO-*d*₆), δ 166.1, 161.8, 157.8, 141.0, 139.9, 134.1, 131.5, 126.9, 126.8, 126.5, 121.9, 61.9, 51.8, 14.5; HRMS(MALDI) *m/z*: calculated for C₁₄H₁₄N₂O₄S₂ 339.0468, found 339.0475 [M + H]⁺.

4.4.16. Methyl 2-((2-methoxycarbonyl)phenyl)disulfanyl)-1H-imidazole-4-carboxylate (3-16**)**

Yield 89%; m.p.: 114–116 °C; yellow solid; ¹H NMR (400 MHz, DMSO-*d*₆), δ 8.35 (d, *J* = 8.2 Hz, 1H, ArH), 8.00 (d, *J* = 7.8 Hz, 1H, ArH), 7.95 (s, 1H, NHCH), 7.76 (t, *J* = 7.8 Hz, 1H, ArH), 7.41 (t, *J* = 7.5 Hz, 1H, ArH), 3.87 (s, 3H, OCH₃), 3.74 (s, 3H, OCH₃); ¹³C NMR (101 MHz, DMSO-*d*₆), δ 158.9, 137.8, 134.2, 131.9, 129.6, 128.9, 127.8, 126.9, 125.2, 124.4, 53.2, 52.4; HRMS(MALDI) *m/z*: calculated for C₁₃H₁₂N₂O₄S₂ 325.0311, found 325.0314 [M + H]⁺.

4.4.17. Methyl 2-((4-chlorophenyl)disulfanyl)-1H-imidazole-4-carboxylate (3-17**)**

Yield 89%; m.p.: 138–140 °C; yellow solid; ¹H NMR (400 MHz, DMSO-*d*₆), δ 8.00 (s, 1H, NHCH), 7.64 (d, *J* = 8.6 Hz, 2H, ArH), 7.49 (d, *J* = 8.7 Hz, 2H, ArH), 3.76 (s, 3H, OCH₃); ¹³C NMR (101 MHz, DMSO-*d*₆), δ 158.7, 147.5, 137.8, 133.5, 129.9, 128.2, 127.9, 125.2, 124.4, 53.2; HRMS(MALDI) *m/z*: calculated for C₁₁H₉ClN₂O₂S₂ 300.9867, found 300.9894 [M + H]⁺.

4.4.18. N-(2-((4-fluorophenyl)disulfanyl)thiazol-5-yl)acetamide (3-18**)**

Yield 95%; m.p.: 119–122 °C; yellow solid; ¹H NMR (400 MHz,

DMSO-*d*₆), δ 11.78 (s, 1H, NH), 7.68 (d, *J* = 8.6 Hz 2H, ArH), 7.50 (s, 1H, CH), 7.32 (t, *J* = 8.3 Hz, 2H, ArH), 2.11 (s, 3H, CH₃); ¹³C NMR (101 MHz, DMSO-*d*₆), δ 167.4, 153.8, 139.4, 132.6, 132.5, 131.5, 128.5, 117.3, 117.1, 22.6; HRMS(MALDI) *m/z*: calculated for C₁₁H₉FN₂OS₂ 300.9934, found 300.9934 [M + H]⁺.

4.4.19. N-(2-((2-nitrophenyl)disulfanyl)thiazol-5-yl)acetamide (3-19**)**

Yield 93%; m.p.: 130–133 °C; yellow solid; ¹H NMR (400 MHz, DMSO-*d*₆), δ 11.76 (s, 1H, NH), 8.41 (d, *J* = 7.9 Hz, 1H, ArH), 8.35 (d, *J* = 8.5 Hz, 1H, ArH), 7.96 (d, *J* = 7.4 Hz, 1H, ArH), 7.61 (t, *J* = 7.4 Hz, 1H, ArH), 7.49 (s, 1H, CH), 2.09 (s, 3H, CH₃); ¹³C NMR (101 MHz, DMSO-*d*₆), δ 167.6, 151.4, 145.3, 139.4, 135.8, 134.8, 128.4, 128.3, 127.8, 126.8, 22.5; HRMS(MALDI) *m/z*: calculated for C₁₁H₉N₃O₃S₂ 327.9879, found 327.9876 [M + H]⁺.

4.4.20. 2-((2-nitrophenyl)disulfanyl)thiazole (3-20**)**

Yield 90%; m.p.: 105–107 °C; yellow solid; ¹H NMR (400 MHz, DMSO-*d*₆), δ 8.37 (d, *J* = 8.2 Hz, 1H, ArH), 8.23 (d, *J* = 8.2 Hz, 1H, ArH), 7.93 (t, *J* = 7.7 Hz, 1H, ArH), 7.87–7.74 (m, 2H, CH), 7.62 (t, *J* = 7.7 Hz, 1H, ArH); ¹³C NMR (101 MHz, DMSO-*d*₆), δ 163.8, 145.6, 144.9, 136.2, 133.9, 128.7, 127.6, 126.9, 124.5; HRMS(MALDI) *m/z*: calculated for C₉H₆N₂O₂S₂ 270.9664, found 270.9663 [M+H]⁺.

4.4.21. 2-(*p*-tolyl)disulfanyl)thiazole (3-21**)**

Yield 75%; m.p.: 60–62 °C; yellow solid; ¹H NMR (400 MHz, CDCl₃), δ 7.80 (d, *J* = 6.1 Hz, 2H, ArH), 7.53 (d, *J* = 7.9 Hz, 2H, ArH), 7.25 (d, *J* = 7.7 Hz, 2H, ArH), 2.30 (s, 3H, CH₃); ¹³C NMR (101 MHz, CDCl₃), δ 136.5, 136.3, 130.2, 129.3, 127.6, 124.9, 21.5; HRMS(MALDI) *m/z*: calculated for C₁₀H₉NS₂ 239.9969, found 239.9970 [M+H]⁺.

4.4.22. 2-((4-fluorophenyl)disulfanyl)thiazole (3-22**)**

Yield 82%; m.p.: 89–91 °C; yellow solid; ¹H NMR (400 MHz, DMSO-*d*₆), δ 8.37 (d, *J* = 8.2 Hz, 1H, ArH), 8.23 (d, *J* = 8.2 Hz, 1H, ArH), δ 7.66 (d, *J* = 8.7 Hz, 2H, ArH), 7.52 (d, *J* = 8.7 Hz, 2H, ArH); ¹³C NMR (101 MHz, DMSO-*d*₆), δ 144.9, 132.7, 132.6, 130.6, 125.0, 123.9, 117.3, 117.1, 40.1, 39.9, 39.7; HRMS(MALDI) *m/z*: calculated for C₉H₆FN₂S₂ 243.9719, found 243.9721 [M+H]⁺.

4.4.23. 2-((4-bromophenyl)disulfanyl)thiazole (3-23**)**

Yield 80%; m.p.: 92–94 °C; yellow solid; ¹H NMR (400 MHz, DMSO-*d*₆), δ 7.61 (d, *J* = 8.5 Hz, 2H, ArH), 7.48 (d, *J* = 8.5 Hz, 2H, ArH), 7.30 (s, 1H, NCH), 6.99 (d, *J* = 4.3 Hz, 1H, SCH); ¹³C NMR (101 MHz, DMSO-*d*₆), δ 134.9, 132.3, 129.2, 121.9, 114.2, 99.4; HRMS(MALDI) *m/z*: calculated for C₉H₆BrN₂S₂ 303.8918, found

303.8914 [M+H]⁺.

4.4.24. 4-Methyl-2-((2-nitrophenyl)disulfanyl)thiazole (3-24)

Yield 92%; m.p.: 61–63 °C; yellow solid; ¹H NMR (400 MHz, CDCl₃), δ 8.36 (d, *J* = 8.2 Hz, 1H, ArH), 8.20 (d, *J* = 8.2 Hz, 1H, ArH), 8.01–7.84 (m, 1H, ArH), 7.64–7.53 (m, 1H, ArH), 7.33 (s, 1H, CH), 2.33 (s, 3H, CH₃); ¹³C NMR (101 MHz, CDCl₃), δ 162.8, 154.6, 145.7, 136.0, 133.9, 128.7, 127.6, 126.9, 118.4, 17.3; HRMS(MALDI) *m/z*: calculated for C₁₀H₈N₂O₂S₃ 284.9821, found 284.9823 [M+H]⁺.

4.4.25. Ethyl 2-((4-methylthiazol-2-yl)disulfanyl)benzoate (3-25)

Yield 91%; m.p.: 103–105 °C; yellow solid; ¹H NMR (400 MHz, DMSO-*d*₆), δ 8.09–8.03 (m, 1H, ArH), 8.01 (d, *J* = 7.9 Hz, 1H, ArH), 7.74 (t, *J* = 7.7 Hz, 1H, ArH), 7.45 (t, *J* = 7.5 Hz, 1H, ArH), 7.28 (s, 1H), 4.41 (s, 2H, CH₂CH₃), 2.32 (s, 3H, CH₃), 1.36 (t, *J* = 7.1 Hz, 3H, CH₂CH₃); ¹³C NMR (101 MHz, DMSO-*d*₆), δ 166.2, 156.3, 154.5, 147.4, 138.4, 134.4, 131.8, 127.4, 125.9, 117.6, 62.2, 17.4, 14.5; HRMS(MALDI) *m/z*: calculated for C₁₃H₁₃NO₂S₃ 312.0181, found 312.0188 [M+H]⁺.

4.4.26. Methyl 2-((5-methyl-1,3,4-oxadiazol-2-yl)disulfanyl)benzoate (3-26)

Yield 93%; m.p.: 80–82 °C; yellow solid; ¹H NMR (400 MHz, DMSO-*d*₆), δ 8.14 (d, *J* = 7.4 Hz, 1H, ArH), 8.03 (d, *J* = 6.7 Hz, 1H, ArH), 7.78 (s, 1H, ArH), 7.47 (d, *J* = 6.3 Hz, 1H, ArH), 3.89 (s, 3H, OCH₃), 2.49 (s, 3H, CH₃); ¹³C NMR (101 MHz, DMSO-*d*₆), δ 167.3, 166.7, 161.7, 138.7, 134.4, 131.6, 127.4, 127.1, 126.5, 53.3, 11.3; HRMS(MALDI) *m/z*: calculated for C₁₁H₁₀N₂O₃S₂ 283.0206, found 283.0209 [M+H]⁺.

4.4.27. Ethyl 2-((5-methyl-1,3,4-oxadiazol-2-yl)disulfanyl)benzoate (3-27)

Yield 88%; m.p.: 73–74 °C; yellow solid; ¹H NMR (400 MHz, DMSO-*d*₆), δ 8.14 (d, *J* = 8.0 Hz, 1H, ArH), 8.04 (d, *J* = 7.7 Hz, 1H, ArH), 7.78 (t, *J* = 7.8 Hz, 1H, ArH), 7.46 (t, *J* = 7.5 Hz, 1H, ArH), 4.35 (q, *J* = 7.1 Hz, 2H, CH₂CH₃), 2.50 (s, 3H, CH₃), 1.34 (t, *J* = 7.1 Hz, 3H, CH₂CH₃); ¹³C NMR (101 MHz, DMSO-*d*₆), δ 167.3, 166.3, 161.7, 138.6, 134.3, 131.6, 127.4, 126.5, 62.2, 14.5, 11.3; HRMS(MALDI) *m/z*: calculated for C₁₂H₁₂N₂O₃S₂ 297.0362, found 297.0365 [M+H]⁺.

4.4.28. 2-Methyl-5-((2-nitrophenyl)disulfanyl)-1,3,4-oxadiazole (3-28)

Yield 92%; m.p.: 91–93 °C; yellow solid; ¹H NMR (400 MHz, DMSO-*d*₆), δ 8.34 (d, *J* = 8.2 Hz, 1H, ArH), 8.30 (d, *J* = 8.2 Hz, 1H, ArH), 7.97 (t, *J* = 7.7 Hz, 1H, ArH), 7.63 (t, *J* = 7.7 Hz, 1H, ArH), 2.51 (s, 3H, CH₃); ¹³C NMR (101 MHz, DMSO-*d*₆), δ 167.5, 161.2, 145.4, 135.9, 134.0, 128.7, 128.1, 126.8, 11.3; HRMS(MALDI) *m/z*: calculated for C₉H₇N₃O₃S₂ 270.0002, found 270.0000 [M+H]⁺.

4.4.29. Methyl 2-((1,3,4-oxadiazol-2-yl)disulfanyl)benzoate (3-29)

Yield 87%; m.p.: 99–101 °C; yellow solid; ¹H NMR (400 MHz, DMSO-*d*₆), δ 9.37 (s, 1H, CH), 8.14 (d, *J* = 8.2 Hz, 1H, ArH), 8.05 (d, *J* = 7.8 Hz, 1H, ArH), 7.87 (t, *J* = 7.8 Hz, 1H, ArH), 7.48 (t, *J* = 7.7 Hz, 1H, ArH), 3.91 (s, 3H, OCH₃); ¹³C NMR (101 MHz, DMSO-*d*₆), δ 166.8, 162.3, 157.5, 138.5, 134.5, 131.7, 127.5, 127.2, 126.6, 53.3; HRMS(MALDI) *m/z*: calculated for C₁₀H₈N₂O₃S₂ 290.9869, found 290.9868 [M+H]⁺.

4.4.30. Methyl 2-((4-methyloxazol-2-yl)disulfanyl)benzoate (3-30)

Yield 90%; m.p.: 68–70 °C; yellow solid; ¹H NMR (400 MHz, DMSO-*d*₆), δ 8.16 (d, *J* = 8.0 Hz, 1H, ArH), 8.04 (d, *J* = 7.7 Hz, 1H, ArH), 7.97 (s, 1H, CH), 7.88 (t, *J* = 7.2 Hz, 1H, ArH), 7.45 (t, *J* = 7.2 Hz, 1H, ArH), 3.90 (s, 3H, OCH₃), 2.07 (s, 3H, CH₃); ¹³C NMR (101 MHz, DMSO-*d*₆), δ 166.7, 139.6, 139.3, 138.8, 134.3, 131.6, 127.2, 126.9, 126.4, 53.2, 11.7; HRMS(MALDI) *m/z*: calculated for C₁₂H₁₁NO₃S₂ 282.0253, found 282.0257 [M+H]⁺.

4.4.31. 2-((4-chlorophenyl)disulfanyl)-1,3,4-oxadiazole (3-31)

Yield 90%; m.p.: 69–72 °C; yellow solid; ¹H NMR (400 MHz, DMSO-*d*₆), δ 9.46 (s, 1H, CH), 7.71 (d, *J* = 8.5 Hz, 2H, ArH), 7.54 (d, *J* = 8.3 Hz, 2H, ArH); ¹³C NMR (101 MHz, DMSO-*d*₆), δ 157.7, 134.7, 133.8, 132.5, 131.4, 130.1; HRMS(MALDI) *m/z*: calculated for C₈H₅ClN₂O₂S₂ 261.9871, found 261.9872 [M + NH₄]⁺.

4.4.32. 4,6-Dimethyl-2-((2-nitrophenyl)disulfanyl)pyrimidine (3-32)

Yield 94%; m.p.: 151–153 °C; yellow solid; ¹H NMR (400 MHz, DMSO-*d*₆), δ 8.34 (d, 6.5 Hz, 1H, ArH), 7.99–7.69 (m, 2H, ArH), 7.55 (d, *J* = 8.4 Hz, 1H, ArH), 7.12 (d, *J* = 25.8 Hz, 1H, ArH), 2.35 (s, 6H, CH₃); ¹³C NMR (101 MHz, DMSO-*d*₆), δ 168.7, 168.3, 135.5, 128.5, 128.0, 127.4, 127.0, 126.3, 118.7, 118.1, 23.8; HRMS(MALDI) *m/z*: calculated for C₁₂H₁₁N₃O₂S₂ 294.0365, found 294.0364 [M + H]⁺.

4.4.33. 2-((4-chlorophenyl)disulfanyl)-4,6-dimethylpyrimidine (3-33)

Yield 80%; m.p.: 84–86 °C; yellow solid; ¹H NMR (400 MHz, DMSO-*d*₆), δ 7.60 (d, *J* = 8.6 Hz, 2H, ArH), 7.44 (d, *J* = 8.6 Hz, 2H, ArH), 7.14 (s, 1H, ArH), 2.40 (s, 6H, CH₃); ¹³C NMR (101 MHz, DMSO-*d*₆), δ 168.6, 167.8, 135.6, 133.1, 130.9, 129.6, 118.4, 23.8; HRMS(MALDI) *m/z*: calculated for C₁₂H₁₁ClN₂S₂ 283.0125, found 283.0130 [M + H]⁺.

4.4.34. 2-((4-bromophenyl)disulfanyl)-4,6-dimethylpyrimidine (3-34)

Yield 84%; m.p.: 76–79 °C; yellow solid; ¹H NMR (400 MHz, DMSO-*d*₆), δ 7.53 (dd, *J* = 15.6, 7.2 Hz, 4H, ArH), 7.15 (s, 1H, ArH), 2.38 (s, 6H, CH₃); ¹³C NMR (101 MHz, DMSO-*d*₆), δ 168.6, 167.7, 136.1, 132.5, 131.0, 121.5, 118.4, 23.8; HRMS(MALDI) *m/z*: calculated for C₁₂H₁₁BrN₂S₂ 326.9620, found 326.9622 [M + H]⁺.

4.4.35. 4,6-Dimethyl-2-(phenyldisulfanyl)pyrimidine (3-35)

Yield 81%; m.p.: 61–63 °C; yellow solid; ¹H NMR (400 MHz, DMSO-*d*₆), δ 7.67 (t, *J* = 8.0 Hz, 2H, ArH), 7.60–7.31 (m, 3H, ArH), 7.22 (s, 1H, ArH), 2.48 (s, 6H, CH₃); ¹³C NMR (101 MHz, DMSO-*d*₆), δ 168.6, 130.9, 129.7, 129.6, 129.2, 128.3, 118.4, 23.8; HRMS(MALDI) *m/z*: calculated for C₁₂H₁₂N₂S₂ 249.0515, found 249.0515 [M + H]⁺.

4.4.36. 4,6-Dimethyl-2-(*p*-tolyl)disulfanyl)pyrimidine (3-36)

Yield 84%; m.p.: 72–75 °C; yellow solid; ¹H NMR (400 MHz, DMSO-*d*₆), δ 7.50 (d, *J* = 8.2 Hz, 2H, ArH), 7.18 (d, *J* = 8.0 Hz, 2H, ArH), 7.12 (s, 1H, ArH), 2.40 (s, 6H, CH₃), 2.28 (s, 3H, CH₃); ¹³C NMR (101 MHz, DMSO-*d*₆), δ 168.4, 138.4, 133.1, 131.6, 130.3, 130.2, 118.2, 23.86, 21.1; HRMS(MALDI) *m/z*: calculated for C₁₃H₁₄N₂S₂ 263.0671, found 263.0674 [M + H]⁺.

4.4.37. 2-((2-nitrophenyl)disulfanyl)pyrimidine (3-37)

Yield 86%; m.p.: 130–132 °C; yellow solid; ¹H NMR (400 MHz, DMSO-*d*₆), δ 8.63 (s, 2H, ArH), 8.31 (d, *J* = 8.1 Hz, 2H, ArH), 7.96 (s, 1H, ArH), 7.59 (s, 1H, ArH), 7.38 (s, 1H, ArH), 7.17 (s, 1H, ArH); ¹³C NMR (101 MHz, DMSO-*d*₆), δ 169.4, 158.6, 136.3, 134.3, 128.1, 126.7, 125.9, 118.9, 99.9; HRMS(MALDI) *m/z*: calculated for C₁₀H₇N₃O₂S₂ 265.0052, found 266.0053 [M + H]⁺.

4.4.38. 2-((4-chlorophenyl)disulfanyl)pyrimidine (3-38)

Yield 80%; m.p.: 79–80 °C; yellow solid; ¹H NMR (400 MHz, DMSO-*d*₆), δ 8.66–8.47 (m, 2H), 7.47 (t, *J* = 9.0 Hz, 2H), 7.29–7.16 (m, 2H), 7.07 (d, *J* = 4.9 Hz, 1H); ¹³C NMR (101 MHz, DMSO-*d*₆), δ 158.0, 134.9, 133.8, 130.2, 129.3, 129.1, 118.3; HRMS(MALDI) *m/z*: calculated for C₁₀H₇ClN₂S₂ 254.9812, found 254.9816 [M + H]⁺.

4.4.39. 2-((4-bromophenyl)disulfanyl)pyrimidine (3-39)

Yield 83%; m.p.: 75–78 °C; yellow solid; ¹H NMR (400 MHz,

DMSO- d_6), δ 8.63 (dd, $J = 22.9, 4.7$ Hz, 2H), 7.43 (dd, $J = 20.0, 12.8$ Hz, 4H), 7.10 (d, $J = 4.0$ Hz, 1H); ^{13}C NMR (101 MHz, DMSO- d_6), δ 158.1, 135.5, 132.0, 130.3, 128.9, 121.8, 118.3; HRMS(MALDI) m/z : calculated for $\text{C}_{10}\text{H}_7\text{BrN}_2\text{S}_2$ 298.9307, found 298.9307 $[\text{M} + \text{H}]^+$.

4.4.40. 2-(*p*-tolylsulfanyl)pyrimidine (**3-40**)

Yield 86%; m.p.: 45–48 °C; yellow solid; ^1H NMR (400 MHz, DMSO- d_6), δ 8.56 (d, $J = 4.9$ Hz, 2H), 7.44 (d, $J = 8.2$ Hz, 2H), 7.13–6.90 (m, 3H), 2.24 (s, 3H, CH_3); ^{13}C NMR (101 MHz, DMSO- d_6), δ 171.2, 157.9, 138.1, 132.9, 129.8, 129.7, 118.0, 21.1; HRMS(MALDI) m/z : calculated for $\text{C}_{11}\text{H}_{10}\text{N}_2\text{S}_2$ 235.0358, found 235.0361 $[\text{M} + \text{H}]^+$.

4.5. In vitro enzyme inhibition assay

The expression and purification of SARS CoV M^{pro} was described by Rao et al. [43]. Basically, the sequence of SARS-CoV M^{pro} cloned into the pGEX-6P-1 vector was transformed into *E. coli* BL21 (DE3) cells. The GST fusion protein, GST-SARS-CoV M^{pro} , was purified by GST-glutathione affinity chromatography, cleaved with PreScission protease, and the recombinant SARS-CoV M^{pro} was further purified by using anion-exchange chromatography. Eventually purified protein was of high purity (>95%) as judged by SDS-PAGE analysis and the concentration is 0.5 μM , and the buffer contains 50 mM Tris-HCl, pH 7.3 and 1 mM EDTA. The fluorogenic substrate with consensus sequence of CoV M^{pro} , MCA-AVLQSGFR-Lys(Dnp)-Lys-NH₂ (95% purity), was synthesized in Shanghai Biological Engineering Company. The substrate was dissolved in DMSO in 0.8 mM liquid storage for use.

The inhibition assay was similar to Yang's procedure [11]. The SARS CoV M^{pro} inhibition assays were conducted by fluorescence resonance energy transfer (FRET). The natural substrate amino acid sequence (AVLQSGFRKK) of SARS-CoV M^{pro} started with the MCA fluorescent group and connected the Dnp fluorescence quenching group with penultimate K. The tested compounds were dissolved by sterilized DMSO and diluted to various concentrations. The settled concentrations of proteins, compounds and substrate were preheated at 37 °C and oscillated. The excitation/emission light was 320/405 nm, and the test was carried out every 5 s for 200 times. Drawing curves, the maximum value of the negative control curve slope is V_0 , and the largest compound curve slope is V_1 . The inhibition ratio can be defined $(1 - V_1/V_0)$. And the IC_{50} value was calculated by equation (1) using GraphPad Prism5:

$$V_0/V = 1 + [I]/\text{IC}_{50} \quad (1)$$

V_0 shows the initial rate of the reaction without inhibitor, V means the initial rate of the reaction with the inhibitor at various concentrations and $[I]$ indicates the concentration of the inhibitor.

The determination of the inhibitor as a valent inhibitor employs the above methods as well, albeit with two modifications. Firstly, the inhibitor concentration was set to 2 or 4 μM . And for each inhibitor concentration, we measured the enzymatic activity of M^{pro} whose concentration spans 0–2 μM . Secondly, M^{pro} and inhibitor were first incubated for 20 min to ensure a thorough 'M^{pro}-inhibitor' reaction and then the inhibition assay was initiated by adding substrate and characterized by fluorescence monitoring.

The further characterization of the inhibitor as a non-competitive inhibitor employs the methods described in earlier work [28]. Basically, the enzymatic velocity of SARS-CoV M^{pro} versus substrate concentrations with presence of inhibitors is depicted by equation (2) [27], where K_i is the dissociation constant for the SARS-CoV M^{pro} complexed with inhibitor **3-31**; factor α reflects the effect of inhibitor **3-31** on the affinity of the enzyme for its substrate; V_{max} and K_m represent the maximum velocity and Michaelis-Menten constant, respectively.

$$v = \frac{V_{\text{max}}[S]}{[S] \left(1 + \frac{[I]}{\alpha K_i} \right) + K_m \left(1 + \frac{[I]}{K_i} \right)} \quad (2)$$

The values of V_{max} and K_m at different inhibitor concentrations were apparent V_{max} and K_m , called $V_{\text{max}}^{\text{app}}$ and K_m^{app} , respectively. According to equation (2), $V_{\text{max}}^{\text{app}}$ and K_m^{app} can be calculated by equation (3).

$$V_{\text{max}}^{\text{app}} = \frac{V_{\text{max}}}{1 + \frac{[I]}{\alpha K_i}}, K_m^{\text{app}} = \frac{K_m \left(1 + \frac{[I]}{K_i} \right)}{1 + \frac{[I]}{\alpha K_i}} \quad (3)$$

The kinetic parameters of $V_{\text{max}}^{\text{app}}$ and K_m^{app} were determined by adding 1 μM SARS-CoV M^{pro} to 20 μM substrate containing varying concentrations of inhibitor 3-31 (0–3 μM). The value of αK_i was then calculated from plots of $1/V_{\text{max}}^{\text{app}}$ versus $1/[I]$. Similarly, the value of K_i was calculated from plots of $V_{\text{max}}^{\text{app}}$ and K_m^{app} versus $1/[I]$.

Mass spectra were recorded on Waters Xevo G2-XS Q-TOF mass spectrometry. Mass spectra were acquired in positive ion mode using a capillary voltage of 3 kV, a sampling cone voltage of 40 V and a source offset voltage of 80 V. The cone gas flow was set up to 50 L/h and desolvation gas flow was 800 L/h. Desolvation temperature and source temperature were set to 400 °C and 100 °C, respectively. The mass of intact protein was obtained by deconvolution of the raw data using MaxEnt1 tool. The samples were prepared at the similar condition with the IC_{50} determination, except that the concentration of the inhibitors was 20 times of the concentration of SARS M^{pro} .

4.6. Molecular docking and comparative field analysis

Chemical structures of the compounds were built within Sybyl 7.3 (Tripos Inc., St Louis, MO). All the molecules were assigned Gasteiger-Hückel charges and minimized by the Tripos force field when convergence reached 0.001 kcal/mol/Å.

Molecular docking of the unsymmetrical aromatic disulfides to the active site of SARS-CoV M^{pro} was performed by FlexX. The crystal structure of SARS-CoV M^{pro} in complex with inhibitor (pdb code 2AMD) was retrieved from the pdb databank. All water molecules were removed, and hydrogen atoms were added in the standard geometry. Any amino acid residue within 6.5 Å of the location of the original inhibitor N9 was considered to be in the binding pocket. Cscore calculation was enabled and set to serial mode. Database docking and subsequent scoring procedures were performed using the default parameters in the program.

For CoMFA, The molecules were superimposed using **3-31** from the molecular docking result as the template. All the parameters were used the default value within CoMFA module and the column filtering was set to 2.0 kcal/mol. The "leave-one-out" (LOO) cross validation method was applied to determine the optimum number of partial least squares (PLS) components. The non-cross validated method was used to derive the final model to explain the quantitative structure-activity relationship in a three dimensional manner.

Acknowledgment

This work was financially supported by the Natural Science Foundation of China (No. 21272128 and 21672114), the "111" Project of Ministry of Education of China (No. B06005) and the National Basic Research Program of China (No. 2013CB734004). We appreciate Professor Chuangzheng Zhou in Nankai University for his kind assistance for the mass spectrometry of SARS CoV main protease.

Appendix A. Supplementary data

Supplementary data related to this article can be found at <http://dx.doi.org/10.1016/j.ejmech.2017.05.045>.

References

- [1] World Health Organization, Summary of Probable SARS Cases with Onset of Illness from 1 November 2002 to 31 July 2003, December 2003. Based on data as of the 31, http://www.who.int/csr/sars/country/table2004_04_21/en/.
- [2] D.H. Goetz, Y. Choe, E. Hansell, Y.T. Chen, M. McDowell, C.B. Jonsson, W.R. Roush, J. McKerrow, C.S. Craik, Substrate specificity profiling and identification of a new class of inhibitor for the major protease of the SARS coronavirus, *Biochemistry* 46 (2007) 8744–8752.
- [3] H. Yang, W. Xie, X. Xue, K. Yang, J. Ma, W. Liang, Q. Zhao, Z. Zhou, D. Pei, J. Ziebuhr, R. Hilgenfeld, K.Y. Yuen, L. Wong, G. Gao, S. Chen, Z. Chen, D. Ma, M. Bartlam, Z. Rao, Design of wide-spectrum inhibitors targeting coronavirus main proteases, *PLoS Biol.* 3 (2005) 1741–1752.
- [4] K. Anand, J. Ziebuhr, P. Wadhvani, J.R. Mesters, R. Hilgenfeld, Coronavirus main proteinase (3CLpro) structure: basis for design of anti-SARS drugs, *Science* 300 (2003) 1763–1767.
- [5] L. Zhou, Y. Liu, W. Zhang, P. Wei, C. Huang, J. Pei, Y. Yuan, L. Lai, Isatin compounds as non-covalent SARS coronavirus 3C-like protease inhibitors, *J. Med. Chem.* 49 (2006) 3440–3443.
- [6] L. Chen, J. Li, C. Luo, H. Liu, W. Xu, G. Chen, O.W. Liew, W. Zhu, C.M. Pua, X. Shen, H. Jiang, Binding interaction of quercetin-3- β -galactoside and its synthetic derivatives with SARS-CoV 3CL^{pro}: structure-activity relationship studies reveal salient pharmacophore features, *Bioorg. Med. Chem.* 14 (2006) 8295–8306.
- [7] R. Ramajayam, K.P. Tan, H.G. Liu, P.H. Liang, Synthesis and evaluation of pyrazolone compounds as SARS-coronavirus 3C-like protease inhibitors, *Bioorg. Med. Chem.* 18 (2010) 7849–7854.
- [8] Y.M. Shao, W.B. Yang, T.H. Kuo, K.C. Tsai, C.H. Lin, A.S. Yang, P.H. Liang, C.H. Wong, Design, synthesis, and evaluation of trifluoromethyl ketones as inhibitors of SARS-CoV 3CL protease, *Bioorg. Med. Chem.* 16 (2008) 4652–4660.
- [9] J. Jacobs, V. Grum-Tokars, Y. Zhou, M. Turlington, S.A. Saldanha, P. Chase, A. Egger, E.S. Dawson, Y.M. Baez-Santos, S. Tomar, A.M. Mielech, S.C. Baker, C.W. Lindsley, P. Hodder, A. Meseccar, S.R. Stauffer, Discovery, synthesis, and structure-based optimization of a series of N-(tert-butyl)-2-(N-arylamido)-2-(pyridin-3-yl) acetamides (ML188) as potent non-covalent small molecule inhibitors of the severe acute respiratory syndrome coronavirus (SARS-CoV) 3CL protease, *J. Med. Chem.* 56 (2013) 534–546.
- [10] P. Thanigaimalai, S. Konno, T. Yamamoto, Y. Koiwai, A. Taguchi, K. Takayama, F. Yakushiji, K. Akaji, S.E. Chen, A. Naser-Tavakolian, A. Schön, E. Freire, Y. Hayashi, Development of potent dipeptide-type SARS-CoV 3CL protease inhibitors with novel P3 scaffolds: design, synthesis, biological evaluation, and docking studies, *Eur. J. Med. Chem.* 68 (2013) 372–384.
- [11] W. Liu, H.M. Zhu, G.J. Niu, E.Z. Shi, J. Chen, B. Sun, W.Q. Chen, H.G. Zhou, C. Yang, Synthesis, modification and docking studies of 5-sulfonyl isatin derivatives as SARS-CoV 3C-like protease inhibitors, *Bioorg. Med. Chem.* 22 (2014) 292–302.
- [12] P. Thanigaimalai, S. Konno, T. Yamamoto, Y. Koiwai, A. Taguchi, K. Takayama, F. Yakushiji, K. Akaji, Y. Kiso, Y. Kawasaki, S.E. Chen, A. Naser-Tavakolian, A. Schön, E. Freire, Y. Hayashi, Design, synthesis, and biological evaluation of novel dipeptide-type SARS-CoV 3CL protease inhibitors: structure-activity relationship study, *Eur. J. Med. Chem.* 65 (2013) 436–447.
- [13] L. Zhang, C.P. Chou, M. Moo-Young, Disulfide bond formation and its impact on the biological activity and stability of recombinant therapeutic proteins produced by *Escherichia coli* expression system, *Biotechnol. Adv.* 29 (2011) 923–929.
- [14] R. Argüello-García, O.N. Medina-Campos, N. Pérez-Hernández, J. Pedraza-Chaverri, G. Ortega-Pierres, Hypochlorous acid scavenging activities of thioallyl compounds from garlic, *J. Agric. Food Chem.* 58 (2010) 11226–11233.
- [15] H.L. Chu, B.S. Wang, P.D. Duh, Effects of selected organosulfur compounds on melanin formation, *J. Agric. Food Chem.* 57 (2009) 7072–7077.
- [16] S. Otto, Dynamic molecular networks: from synthetic receptors to self-replicators, *Acc. Chem. Res.* 45 (2012) 2200–2210.
- [17] E. Turos, K.D. Revell, P. Ramaraju, D.A. Gergeres, K. Greenhalgh, A. Young, N. Sathyanarayan, S. Dickey, D. Lim, M.M. Alhamadsheh, K. Reynolds, Unsymmetric aryl-alkyl disulfide growth inhibitors of methicillin-resistant *Staphylococcus aureus* and *Bacillus anthracis*, *Bioorg. Med. Chem.* 16 (2008) 6501–6508.
- [18] T.R. DiRaimondo, N.M. Plugis, X. Jin, C. Khosla, Selective inhibition of extracellular thioredoxin by asymmetric disulfides, *J. Med. Chem.* 56 (2013) 1301–1310.
- [19] K.J. Choi, Y.G. Yu, H.G. Hahn, J.D. Choi, M.Y. Yoon, Characterization of aceto-hydroxyacid synthase from *Mycobacterium tuberculosis* and the identification of its new inhibitor from the screening of a chemical library, *FEBS Lett.* 579 (2005) 4903–4910.
- [20] K.J. Choi, K.M. Noh, D.E. Kim, B.H. Ha, E.E. Kim, M.Y. Yoon, Identification of the catalytic subunit of aceto-hydroxyacid synthase in *Haemophilus influenzae* and its potent inhibitors, *Arch. Biochem. Biophys.* 466 (2007) 24–30.
- [21] J. Shang, W.M. Wang, Y.H. Li, H.B. Song, Z.M. Li, J.G. Wang, Synthesis, crystal structure, in vitro aceto-hydroxyacid synthase inhibition, in vivo herbicidal activity, and 3D-QSAR of new asymmetric aryl disulfides, *J. Agric. Food Chem.* 60 (2012) 8286–8293.
- [22] Z.S. Li, W.M. Wang, W. Lu, C.W. Niu, Y.H. Li, Z.M. Li, J.G. Wang, Synthesis and biological evaluation of nonsymmetrical aromatic disulfides as novel inhibitors of aceto-hydroxyacid synthase, *Bioorg. Med. Chem. Lett.* 23 (2013) 3723–3727.
- [23] C.S. Sepúlveda, C.C. García, J.M. Levingston Macleod, N. López, E.B. Damonte, Targeting of arenavirus RNA synthesis by a carboxamide-derivatized aromatic disulfide with virucidal activity, *PLoS One* 8 (2013) e81251.
- [24] H.H. Lara, L. Ixtepan-Turrent, E.N. Garza-Treviño, S.M. Flores-Teviño, G. Borkow, C. Rodríguez-Padilla, Antiviral properties of 5, 5'-dithiobis-2-nitrobenzoic acid and bacitracin against T-tropic human immunodeficiency virus type 1, *Virology* 438 (2011) 137.
- [25] C.C. García, I. Topisirovic, M. Djavani, K.L. Borden, E.B. Damonte, M.S. Salvato, An antiviral disulfide compound blocks interaction between arenavirus Z protein and cellular promyelocytic leukemia protein, *Biochem. Biophys. Res. Commun.* 393 (2010) 625–630.
- [26] M. Han, J.T. Lee, H.G. Hahn, A traceless, one-pot preparation of unsymmetric disulfides from symmetric disulfides through a repeated process involving sulfenic acid and thiosulfinate intermediates, *Tetrahedron. Lett.* 52 (2011) 236–239.
- [27] R. Copeland, Reversible inhibitors, in: R. Copeland, *Enzymes (Eds.), A Practical Introduction to Structure, Mechanism, and Data Analysis*, second ed., Wiley-VCH, Inc., New York, 2000, pp. 266–304.
- [28] F. Wang, C. Chen, X. Liu, K. Yang, X. Xu, H. Yang, Crystal structure of feline infectious peritonitis virus main protease in complex with synergetic dual inhibitors, *J. Virol.* 90 (2015) 1910–1917.
- [29] P.T. Corbett, J. Leclaire, L. Vial, K.R. West, J.L. Wieter, J.K. Sanders, S. Otto, Dynamic combinatorial chemistry, *Chem. Rev.* 106 (2006) 3652–3711.
- [30] T. Christopheit, A. Albert, H.K. Leiros, Discovery of a novel covalent non- β -lactam inhibitor of the metallo- β -lactamase NDM-1, *Bioorg. Med. Chem.* 24 (2016) 2947–2953.
- [31] J. Zhang, H.I. Pettersson, C. Huitema, C. Niu, J. Yin, M.N. James, L.D. Eltis, J.C. Vederas, Design, synthesis, and evaluation of inhibitors for severe acute respiratory syndrome 3C-like protease based on phthalhydrazide ketones or heteroaromatic esters, *J. Med. Chem.* 50 (2007) 1850–1864.
- [32] M. Rarey, B. Kramer, T. Lengauer, G. Klebe, A fast flexible docking method using an incremental construction algorithm, *J. Mol. Biol.* 261 (1996) 470–489.
- [33] J. Wang, H. Tan, Y. Li, Y. Ma, Z. Li, L.W. Guddat, Chemical synthesis, in vitro aceto-hydroxyacid synthase (AHAS) inhibition, herbicidal activity, and computational studies of isatin derivatives, *J. Agric. Food Chem.* 59 (2011) 9892–9900.
- [34] G. Jug, M. Anderluh, T. Tomašič, Comparative evaluation of several docking tools for docking small molecule ligands to DC-SIGN, *J. Mol. Model.* 21 (2015) 164.
- [35] R.K. Mishra, J. Singh, A structure guided QSAR: a rapid and accurate technique to predict IC₅₀: a case study, *Curr. Comput. Aided Drug Des.* 11 (2015) 152–163.
- [36] H. Liu, Q. Shen, J. Zhang, W. Fu, Evaluation of various inverse docking schemes in multiple targets identification, *J. Mol. Graph. Model.* 29 (2010) 326–330.
- [37] X. Hou, J. Du, J. Zhang, L. Du, H. Fang, M. Li, How to improve docking accuracy of AutoDock4.2: a case study using different electrostatic potentials, *J. Chem. Inf. Model.* 53 (1) (2013 Jan 28) 188–200.
- [38] A.C. Wallace, R.A. Laskowski, J.M. Thornton, LIGPLOT: a program to generate schematic diagrams of protein-ligand interactions, *Protein Eng.* 8 (1995) 127–134.
- [39] R.D. Cramer, D.E. Patterson, J.D. Bunce, Comparative molecular field analysis (CoMFA). 1. Effect of shape on binding of steroids to carrier proteins, *J. Am. Chem. Soc.* 110 (1988) 5959–5967.
- [40] D.P. Jiang, C.C. Zhu, X.S. Shao, J.G. Cheng, Z. Li, Bioactive conformation analysis of anthranilic diamide insecticides: DFT-based potential energy surface scanning and 3D-QSAR investigations, *Chin. Chem. Lett.* 26 (2015) 662–666.
- [41] X.L. Yue, H. Li, S.S. Liu, Q.Y. Zhang, J.J. Yao, F.Y. Wang, N-Fluorinated phenyl-N'-pyrimidyl urea derivatives: synthesis, biological evaluation and 3D-QSAR study, *Chin. Chem. Lett.* 25 (2014) 1069–1072.
- [42] C.A. Lipinski, F. Lombardo, B.W. Dominy, P.J. Feeney, Experimental and computational approaches to estimate solubility and permeability in drug discovery and development settings, *Adv. Drug Deliv. Rev.* 46 (2001) 3–26.
- [43] H. Yang, M. Yang, Y. Ding, Y. Liu, Z. Lou, Z. Zhou, L. Sun, L. Mo, S. Ye, H. Pang, G.F. Gao, K. Anand, M. Bartlam, R. Hilgenfeld, Z. Rao, The crystal structures of severe acute respiratory syndrome virus main protease and its complex with an inhibitor, *Proc. Natl. Acad. Sci. U. S. A.* 100 (2003) 13190–13195.